Available on CMS information server

CMS NOTE 2002/XXX

The Compact Muon Solenoid Experiment

CMS Note

Mailing address: CMS CERN, CH-1211 GENEVA 23, Switzerland

April 2002

Jet energy correction using weights on calorimeter longitudinal readouts

O.Kodolova, I.Vardanian

Moscow State University, Moscow, Russia

A.Oulianov

ITEP, Moscow, Russia

S.Kunori

University of Maryland, USA

Abstract

Jet energy corrections were performed by means of an optimization of the relative weights for longitudinally segmented calorimeter readouts in addition to an overall energy scale factor. Two different procedures have been investigated. Both procedures reproduced an improvement in energy scale provided by a previous correction procedure with an overall energy scale, but failed to improve the jet energy resolution significantly.

1 Introduction

The CMS calorimeter has been designed for precise energy measurements of photons and electrons in the psuedorapidity interval $|\eta| < 2.6$, and moderate precision energy measurements of quarks and gluons in $|\eta| < 5.0$ through the measurement of jets of particles [1, 2, 3]. The central calorimeter ($\eta < 3$) consists of PbWO4 crystals for the electromagnetic calorimeter (ECAL) and scintillator-brass (70% Cu, 30% Zn) sampling calorimeter for the hadron calorimeter (HCAL). The response of the calorimeter to photons is quite linear versus incident energy, while the response to hadrons depends strongly on incident energy[4]. This quite different response of the calorimeter to photons and hadrons leads to a nonlinear response of the calorimeter to jet energy and a smearing effect in the energy resolution. Since the calorimeter response depends on the energy of a jet (not the transverse energy), the transverse energy scale of jets showed a strong psuedorapidity dependence.

In order to restore the transverse energy scale for reconstructed jets, a previous CMS study [5] used a simple correction function which depended only on transverse energy (E_T) and pseudorapidity (η). Since this approach corrected the energy scale by simply multiplying by a correction factor, it did not improve the energy resolution for individual jets, but did improve trigger turn on curves [5] and reconstruction of dijet masses [6] by equalizing the jet energy scale in the whole range of η in the detector.

This note describes further attempts to improve both the jet energy scale and the energy resolution by optimizing relative weights between ECAL, HAC1 (first longitudinal segment in hadron calorimeter) and HAC2 (second segments) in addition to applying an overall scale factor. ECAL has a single readout in longitudinal direction (25X0, 1.1λ). HAC1 is a single layer of scintillator placed on the front face of HCAL and HAC2 is the rest of HCAL. Two methods have been tried which differed in their optimization procedure. Also, the two analysis used different Mote Carlo data samples and different software packages for jet reconstruction. In the following sections, we describe the optimization procedure and results from the two analysis.

2 Analysis-1

The first analysis used a FORTRAN program within the CMSIM framework to reconstruct jets. The event sample was generated using CMKIN with Pythia 6, and the detector simulation was done with CMSIM (version 120).

2.1 Generated event sample

Samples of QCD jet events at energy $\sqrt{s} = 14$ TeV were generated in different P_T intervals [CKIN(3),CKIN(4)] with Pythia 6.152 [7] using Pythia parameter settings adopted in [8]. The parameters included:

- The parton density structure function CTEQ 5L,
- Pythia generation datacards (Table 1).

Table 1: Pythia generation datacards for QCD event sample.

MSEL = 1	Non-diffractive (jet) processes
MSTP(2) = 2	2nd order running of α_s
MSTP(33) = 3	K-factors: fixed and α_s scale shift at PARP(33) = 0.075 * Q^2
MSTP(82) = 4	Multi-parton interactions switched on
MSTP(81) = 1	Multi-parton interactions switched on
PARP(82) = 3.2	regularization scale $p_{\perp 0}$ of the transverse momentum spectrum for multiple interaction with MSTP(82) ≥ 2

2.2 Calorimeter simulation with CMSIM

CMS calorimeter responses were simulated using GEANT3 with detailed calorimeter geometry descriptions (CMSIM120 [9]). Barrel and endcap regions of the calorimeter were considered. The calorimeter is segmented into projective towers pointing at the interaction point, and the fine-grained structure of the ECAL is not used in this analysis. In all of the barrel and most of the endcap regions, the size of a tower is $\Delta\eta = 0.0870$ by $\Delta\varphi = 2\pi/72 \approx 0.0873$. At high η in the endcap region ($\eta > 1.74$), the towers become larger in η, but keep the same size in φ. The scintillator layers are combined in 4 readouts in depth in the barrel (layer 1(HB1), layers 2-15(HB2), layer 16(HB3), outer calorimeter(HB4)) and 2 readouts (layer 1(HE1), layers 2-20(HE2)) in the endcap [11]. Note that the longitudinal segmentation in the barrel HCAL in CMSIM had additional segmentation compared to the actual readouts. This CMSIM feature was used to determine longitudinal weights which could be built into the hardware, e.g. optical filter in optical signal path in HCAL.

For the ECAL signal, electronics noise of 0.03 GeV (E_T/crystal) and 0.150 GeV (E/crystal) in sigma were added, and energy thresholds of 0.03 GeV (E_T/crystal) and 0.150 GeV (E/crystal) were applied in the barrel and endcap region respectively. Noise in the hadronic calorimeter readouts was not considered.

For the initial energy scale of the HCAL signal, the sampling weights shown in Table 2 were used. These weights were determined using GHEISHA for $E_T = 50$ GeV pions at $0.05 < \eta < 0.3$ for the barrel and $1.8 < \eta < 2.2$ for the endcap part of calorimeters. The GEANT CUTS were 1 MeV for electrons and gammas and 10 MeV for hadrons.

Table 2: Default calibration constants for hadron calorimeter.

Barrel:	118E5	147E5	147E5	150E5
Endcap:	156E5	220E5	220E5	

2.3 QCD jet reconstruction

Generator-level jets were reconstructed with a simple cone algorithm PYCELL using two different cone radii 0.5 and 1.0. All stable particles including muons and neutrinos from Pythia were used. Calorimeter-level jets were reconstructed with corresponding cone radii of 0.5 and 1.0 with a modified window type algorithm [10] using calorimeter energies determined using the default calibration constants shown in Table 2. Pile-up effects from minimum bias events were not considered.

2.4 Optimization of weights

Transverse energies of jets were reconstructed from the energies deposited in the electomagnetic calorimeter (ECAL) and hadronic calorimeter readout layers (HB1,HB2,HB3,HB4-barrel and HE1,HE2-endcap) using the following equation:

$$E^{rec}_{Tjet_i} = \alpha \times E^{ECAL}_T + \sum \beta_j \times HB_j + \sum \gamma_j \times HE_j \tag{1}$$

where $\alpha, \beta_j, \gamma_j$ are the additional weights for the calorimeter depth segmentation and depend on E_T and η. These weights were optimized by minimizing two different functionals:

$$S1 = \sqrt{\frac{\sum(E^{rec}_{Tjet_i} - E^{gen}_{Tjet_i})^2}{nevent - 1}} \tag{2}$$

$$S2 = \frac{S1}{< \frac{E^{rec}_{Tjet_i}}{E^{gen}_{Tjet_i}} >} \tag{3}$$

The energy resolution dependence on transverse energy of the generator-level jets for both functionals is presented in Fig.1-6 for three different pseudorapidity regions and the two cone sizes. The same dependence for the case of the default calibration coefficients is shown for comparison. No significant improvement of resolution is observed.

Concerning the relative error, as defined in equation 4, one can see in Figs. 7-12 that the linearity of the jet energy scale is restored. The best result was obtained by optimizing with function 3.

$$Relative\ error = \frac{< E_{Tjet}^{gen} - E_{Tjet}^{rec} >}{< E_{Tjet}^{rec} >} \quad (4)$$

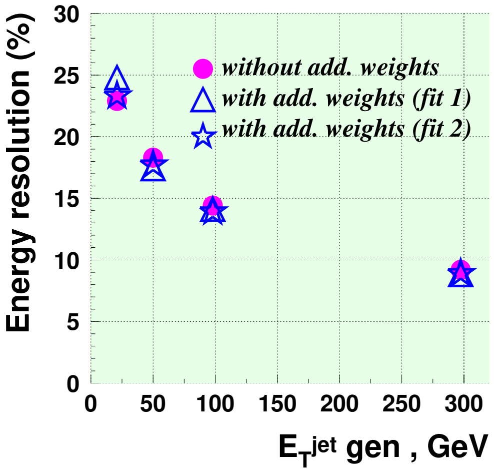

Figure 1: Energy resolution as a function of E_T of particle-level jets in pseudorapidity interval $\eta < 0.3$ and R=0.5.

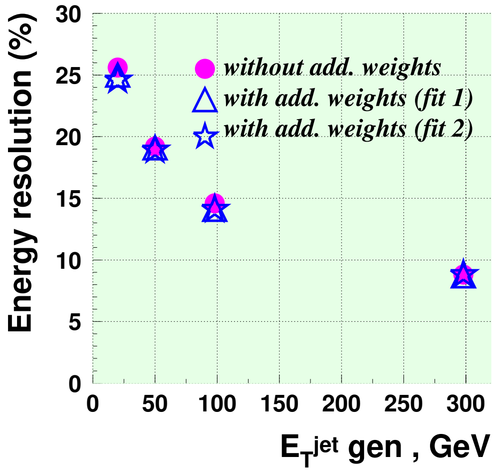

Figure 2: Energy resolution as a function of E_T of particle-level jets in pseudorapidity interval $0.6 < \eta < 0.8$ and R=0.5.

3 Analysis-2

This analysis used a jet reconstruction program in ORCA [13]. The QCD jet event sample was produced with the CMSIM116 detector simulation package and digitized with ORCA4 (HLT sample from spring 2000 production).

The optimization procedure of calorimeter longitudinal weights is described in sec 3.4. These weights are optimized to result in a best QCD jet energy resolution at different values of jet energies.

3.1 Calorimeter simulation

The QCD event sample was generated with Pythia 6 and processed through CMSIM116 for calorimeter simulation with GEANT3. The main difference between CMSIM120 used in Analysis-1 and CMS116 used in Analysis-2 was the weight for the first layer in the barrel (HB) and endcap (HE). CMSIM120 had an additional overweight factor of 1.6 for e/pi compensation for hadronic showers starting in ECAL[12]. This difference was removed by rescaling CMS116 energy during jet reconstruction as described later.

3.2 Calorimeter readout segmentation in ORCA

In ORCA4, the longitudinal readouts in HCAL were regrouped from the segmentation in CMSIM. In the barrel, they were grouped to HB1 (a single scintillator layer before the HCAL absorber), HB2 (main HCAL segment with 14 scintillator layers), HB3 (a segment behind the crack in the HB/HE interface region) and HB4 (Hadron Outer calorimeter). In the endcap, the segments were HE1 (single scintillator layer before the HCAL absorber) and HE2 (main segment).

Electromagnetic and hadron calorimeter readouts are grouped into towers of $\Delta\eta \times \Delta\phi = .087 \times .087$ in the barrel and most of the endcap. For $|\eta| > 1.74$, the phi granularity increased to 0.174.

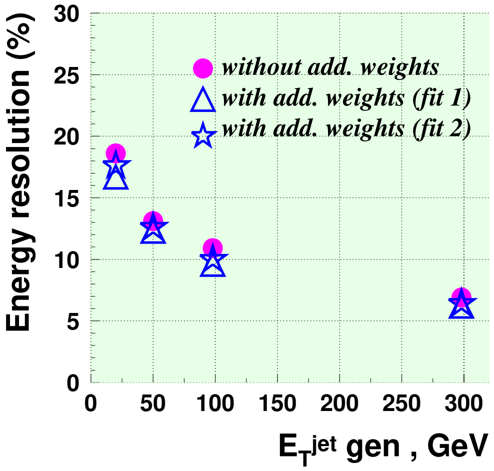

Figure 3: Energy resolution as a function of E_T of particle-level jets in pseudorapidity interval $1.8 < \eta < 2.1$ and R=0.5.

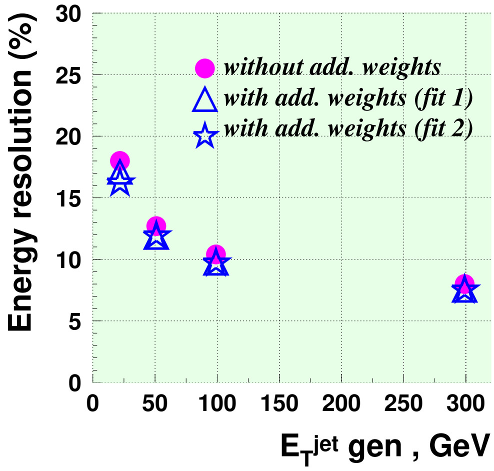

Figure 4: Energy resolution as a function of E_T of particle-level jets in pseudorapidity interval $\eta < 0.3$ and R=1.

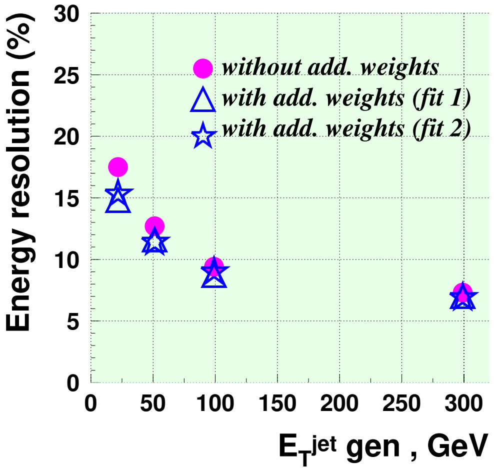

Figure 5: Energy resolution as a function of E_T of particle-level jets in pseudorapidity interval $0.6 < \eta < 0.8$ and R=1.

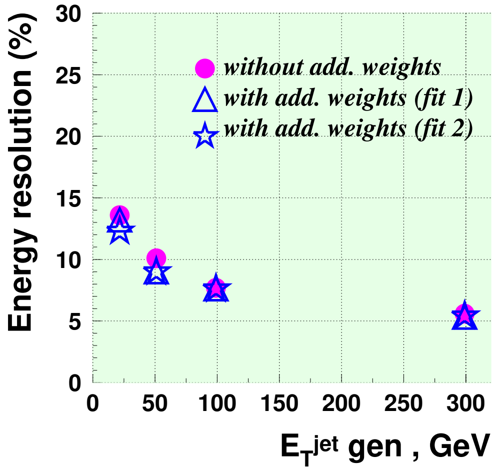

Figure 6: Energy resolution as a function of E_T of particle-level jets in pseudorapidity interval $1.8 < \eta < 2.1$ and R=1.

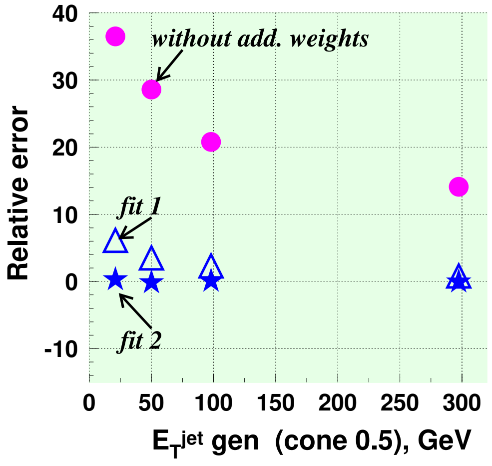

Figure 7: Difference (in percent) between E_T of particle-level jets and calorimeter-level jets in pseudorapidity interval $\eta < 0.3$ and R=0.5.

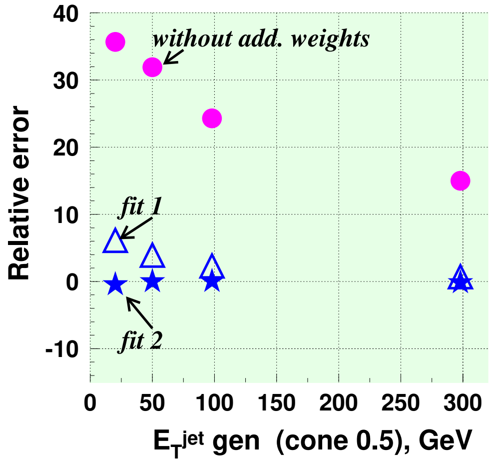

Figure 8: Difference (in percent) between E_T of particle-level jets and calorimeter-level jets in pseudorapidity interval $0.6 < \eta < 0.8$ and R=0.5.

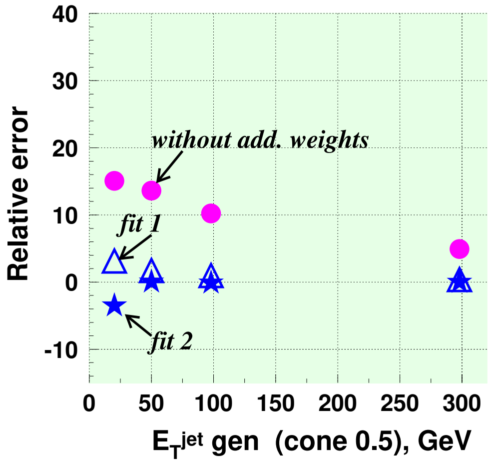

Figure 9: Difference (in percent) between E_T of particle-level jets and calorimeter-level jets in pseudorapidity interval $1.8 < \eta < 2.1$ and R=0.5.

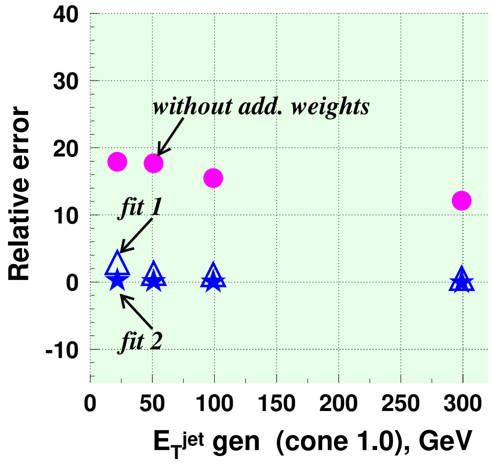

Figure 10: Difference (in percent) between E_T of particle-level jets and calorimeter-level jets in pseudorapidity interval $\eta < 0.3$ and R=1.

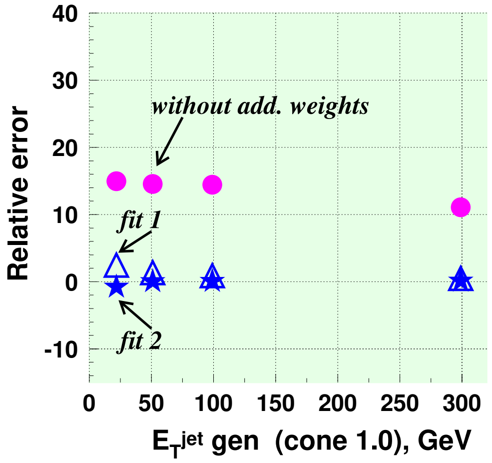

Figure 11: Difference (in percent) between E_T of particle-level jets and calorimeter-level jets in pseudorapidity interval $0.6 < \eta < 0.8$ and R=1.

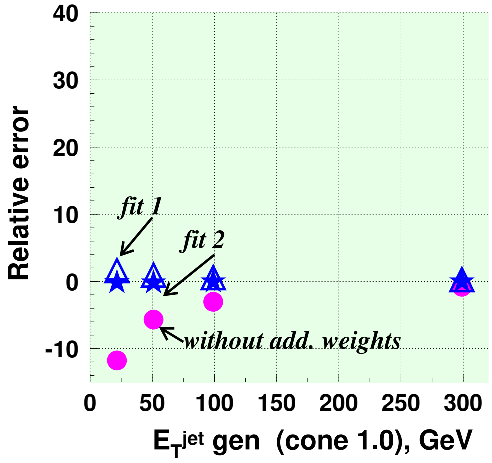

Figure 12: Difference (in percent) between E_T of particle-level jets and calorimeter-level jets in pseudorapidity interval $1.8 < \eta < 2.1$ and R=1.

Table 3: Noise levels per readout channel and digi thresholds. HCAL noise is to be scaled by the calibration factors of 120-220 and corresponds to 70-130 MeV per readout.

Subsystem	Noise level	Digi threshold
ECAL Barrel	30 MeV	60 MeV
ECAL Endcap	150 MeV	300 MeV
HCAL	0.6 MeV	300 MeV

The noise levels and digi thresholds used in readout simulation are listed in Table 3. No additional tower threshold was used.

3.3 QCD jet reconstruction

Level 2 trigger jets (also called off-line jets in this note) are reconstructed by using jet finding algorithms on calorimeter tower signals. Jet energies and momenta reconstructed in different depth compartments in different parts of the calorimeter (i.e. EB, EE, HB1, HB2, HB3 HB4, HE1 and HE2) are saved separately. HCAL energies and momenta are then rescaled with the new calibration factors used in CMSIM120 in order to remove differences in initial energy scales between CMSIM116 and CMS120 production. Finally additional weights w_i are applied to different readouts. The reconstructed jet 4-momentum is calculated as

$$P_{\mathrm{rec}} = w_{\mathrm{EB}} P_{\mathrm{EB}} + w_{\mathrm{HB1}} P_{\mathrm{HB1}} + w_{\mathrm{HB2}}(P_{\mathrm{HB2}} + P_{\mathrm{HB3}} + P_{\mathrm{HB4}}) + w_{\mathrm{EE}} P_{\mathrm{EE}} + w_{\mathrm{HE1}} P_{\mathrm{HE1}} + w_{\mathrm{HE2}} P_{\mathrm{HE2}} \quad (5)$$

A common additional weight is used for HB2, HB3, HB4 readouts.

3.4 Optimization of weights

QCD di-jet data samples at low luminosity ($10^{33}\mathrm{cm}^{-2}\mathrm{s}^{-1}$) were used in this study. The ORCA standard iterative cone algorithm with the cone size $R = 0.5$ and the seed value E_T =1 GeV was used to find both generator particle level jets (including in-time pile-up particles) and off-line calorimeter level jets. Off-line jets were then matched to generator particle level jets if $\Delta R = \sqrt{\Delta\eta^2 + \Delta\phi^2} < 0.2$. This requirement is

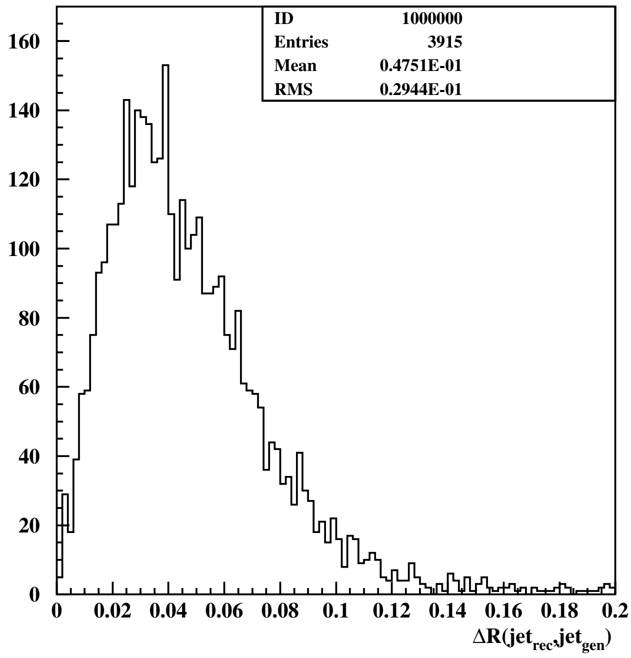

Figure 13: Distribution of the distance $\Delta R = \sqrt{\Delta\eta^2 + \Delta\phi^2}$ between a generator level jet and a best matching calorimeter jet for 70 GeV $< E_{T\,\mathrm{gen}} <$ 110 GeV and $|\eta_{\mathrm{gen}}| < 0.4$.

adequate for high energy jets as can be seen from Fig.13. Particle level jets with no matching calorimeter jet were excluded from further consideration.

Weight optimizations were performed independently at several values of $E_{T\,\mathrm{gen}}$ in several regions of η_{gen}. The optimization procedure for a given jet energy $E_{T\,\mathrm{gen}}^{0}$ consisted of the following steps described in some detail below:

- a set of values for the weights w_i were chosen;
- for this set of weights, jet energy corrections were calculated to set the correct energy scale for off-line jets $< E_{T\,\mathrm{corr}}(E_{T\,\mathrm{rec}}) >= E_{T\,\mathrm{gen}}$ in the vicinity of $E_{T\,\mathrm{gen}}^{0}$;
- energy resolution was calculated for corrected jets;
- these steps were repeated with different values of weights w_i; varying the weights, optimum values w_i^{opt} resulting in a best energy resolution were determined.

Jet energy corrections were calculated in a way similar to that described in [5]. In this analysis the average off-line jet transverse energy $< E_{T\,\mathrm{rec}} >$ as a function of the particle level jet transverse energy $E_{T\,\mathrm{gen}}$ was fitted with a linear function

$$< E_{T\,\mathrm{rec}} >= p1 + p2 \cdot E_{T\,\mathrm{gen}} \tag{6}$$

in the energy region $E_{T\,\mathrm{gen}}^{0} - 20\% < E_{T\,\mathrm{gen}} < E_{T\,\mathrm{gen}}^{0} + 20\%$ as illustrated in Fig.14. The reconstructed jet energy was then corrected in the obvious way

$$E_{T\,\mathrm{corr}} = \frac{E_{T\,\mathrm{rec}} - p1}{p2} \tag{7}$$

Finally, the jet energy resolution was calculated as

$$\mathrm{RESOLUTION} = \frac{\mathrm{RMS}(E_{T\,\mathrm{corr}}/E_{T\,\mathrm{gen}})}{< E_{T\,\mathrm{corr}}/E_{T\,\mathrm{gen}} >} \tag{8}$$

Table 4: Optimum weights and energy resolutions for $E_T = 30$ GeV jets.

η range	EB	HB1	HB2	EE	HE1	HE2	RESOLUTION with simple energy scale corrections	RESOLUTION with optimum weights
0.0-0.4	1.55	0.92	1.15				0.229	0.218
0.4-0.8	1.60	1.03	1.14				0.222	0.211
0.8-1.1	1.65	1.03	1.14				0.213	0.211
1.25-1.45	1.60	1.09	1.36			1.37	0.203	0.200
1.7-2.0				1.67	0.99	1.24	0.196	0.186
2.0-2.4				1.59	0.73	1.22	0.179	0.166

Table 5: Optimum weights and energy resolutions for $E_T = 50$ GeV jets.

η range	EB	HB1	HB2	EE	HE1	HE2	RESOLUTION with simple energy scale corrections	RESOLUTION with optimum weights
0.0-0.4	1.56	1.05	1.11				0.178	0.167
0.4-0.8	1.59	1.02	1.14				0.177	0.166
0.8-1.1	1.61	1.07	1.19				0.174	0.164
1.25-1.45	1.54	0.98	1.40			1.40	0.166	0.160
1.7-2.0				1.57	0.88	1.26	0.157	0.149
2.0-2.4				1.53	0.83	1.20	0.148	0.139

over 20% range of $E_{T\text{gen}}$. Sample jet energy distributions are given in Fig.15-19.

From equations (5) and (7) one can write

$$E_{\text{corr}} = w'_{\text{EB}}E_{\text{EB}} + w'_{\text{HB1}}E_{\text{HB1}} + w'_{\text{HB2}}(E_{\text{HB2}} + E_{\text{HB3}} + E_{\text{HB4}}) + w'_{\text{EE}}E_{\text{EE}} + w'_{\text{HE1}}E_{\text{HE1}} + w'_{\text{HE2}}E_{\text{HE2}}, \quad (9)$$

with jet energy dependent weights w' defined as

$$w'_i = \frac{1 - p1(w)/E_{T\text{rec}}(w)}{p2(w)} \cdot w_i. \quad (10)$$

Substituting the optimum weights w^{opt} into (10) one gets the absolute weights

$$w'^{\text{opt}}_i = \frac{1 - p1/E_{T\text{rec}}}{p2} \cdot w^{\text{opt}}_i \quad (11)$$

which provide both the correct energy scale and the optimum resolution for reconstructed calorimeter jets.

Table 6: Optimum weights and energy resolutions for $E_T = 80$ GeV jets.

η range	EB	HB1	HB2	EE	HE1	HE2	RESOLUTION with simple energy scale corrections	RESOLUTION with optimum weights
0.0-0.4	1.48	1.12	1.12				0.143	0.136
0.4-0.8	1.49	0.95	1.19				0.141	0.134
0.8-1.1	1.49	1.08	1.19				0.144	0.137
1.25-1.45	1.47	0.98	1.40			1.54	0.136	0.133
1.7-2.0				1.44	1.04	1.15	0.134	0.128
2.0-2.4				1.32	1.03	1.15	0.123	0.120

Table 7: Optimum weights and energy resolutions for $E_T = 100$ GeV jets.

η range	EB	HB1	HB2	EE	HE1	HE2	RESOLUTION with simple energy scale corrections	RESOLUTION with optimum weights
0.0-0.4	1.40	1.21	1.15				0.128	0.124
0.4-0.8	1.46	1.19	1.08				0.137	0.129
0.8-1.1	1.43	1.00	1.25				0.131	0.127
1.25-1.45	1.35	1.42	1.42			1.39	0.128	0.125
1.7-2.0				1.44	0.81	1.15	0.131	0.124
2.0-2.4				1.26	1.03	1.14	0.129	0.128

Table 8: Optimum weights and energy resolutions for $E_T = 120$ GeV jets.

η range	EB	HB1	HB2	EE	HE1	HE2	RESOLUTION with simple energy scale corrections	RESOLUTION with optimum weights
0.0-0.4	1.40	0.93	1.16				0.124	0.119
0.4-0.8	1.41	1.13	1.13				0.132	0.126
0.8-1.1	1.40	1.16	1.16				0.125	0.121
1.25-1.45	1.44	0.82	1.37			1.73	0.125	0.119
1.7-2.0				1.37	0.91	1.14	0.122	0.116
2.0-2.4				1.29	0.70	1.17	0.117	0.113

3.5 Results

The optimum readout weights $w_i'^{\mathrm{opt}}$ as defined in (11) are listed in Tables 4-8 for different jet energies and pseudorapidity regions. The jet energy resolutions obtained with the optimum weights and those obtained with the trivial weights $w_i = 1$ and energy scale corrections are also compared in these tables. Relative statistical errors of the listed energy resolution values amount to 3%. Nevertheless, it should be noted that the energy resolutions obtained with different weights from the same samples of jets proved to be correlated. The ratio of energy resolutions obtained with the trivial and optimum weights was estimated to be accurate with 1.5% statistical error. The resulting statistical uncertainty of the optimum weights was estimated to be 5% for EB, EE, HB2, HE2 and 15% for HB1, HE1 readouts.

From these results we can conclude that increasing ECAL weights by 20-50% (depending on jet energy) improves the jet energy resolution by 4% on average.

The optimum readout weights for ECAL tend to increase at lower jet energies as shown in Fig.20, while no clear energy dependence is seen in optimal weights for both readouts in HCAL.

4 Conclusions

Two independent procedures were investigated to improve the jet energy resolution. The procedures optimized relative weights between longitudinally segmented calorimeter readouts in addition to an overall energy scale factor. Both procedures resulted in good jet energy scale and linearity similar to a result from an energy scale correction with one overall scale factor. However they failed to improve the jet energy resolution significantly.

This lack of improvement may be attributed to the relatively thick ECAL compartment (1.1 interaction length) without any longitudinal segmentation. In general, a calorimeter can be divided into three longitudinal sections. The first section measures mainly showers due to photons in a jet, the second section measures a mixture of showers due to photons and hadrons, and the third section measures showers due to hadrons. By optimizing a weight for the second section one can somewhat compensate a different response of calorimeter to photons and hadrons, consequently improving jet energy resolution. The thick ECAL subsumes the second section completely. Therefore, there was not much room to improve the jet energy resolution by optimizing longitudinal calorimeter weights in the CMS calorimeter.

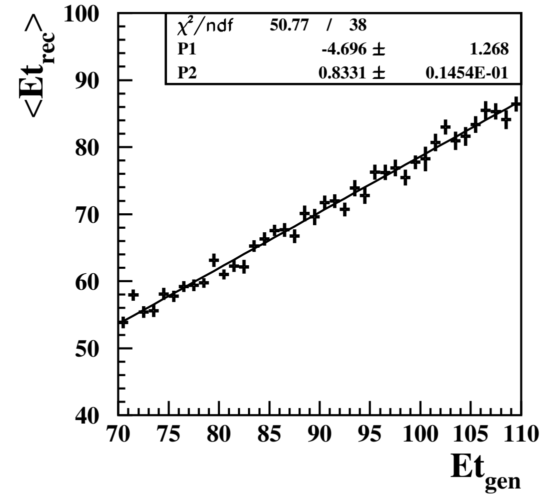

Figure 14: Jet energy scale calibration for ${E_T}^0_{\mathrm{gen}} = 90$ GeV and $|\eta_{\mathrm{gen}}| < 0.4$. The average reconstructed jet energy is fitted as a linear function of generator particle jet energy $< E_{T\mathrm{rec}} >= p1 + p2 \cdot E_{T\mathrm{gen}}$. This plot was made with the weights $w_i = 1$. The same method was used to calibrate jet energy scale for each set of weights w_i used in the optimization procedure.

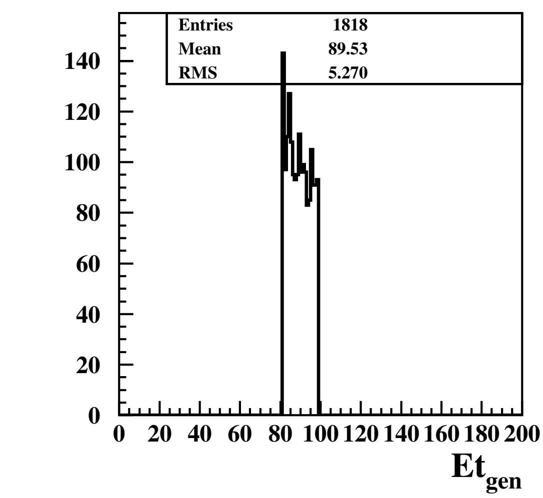

Figure 15: Energy distribution of the particle jets used in the weight optimization for 90 GeV jets with $|\eta| < 0.4$.

5 Acknowledgments

We are thankful to L.Sarycheva, N.Kruglov, A.Demianov and A.Gribushin for useful discussions, and V.Gavrilov for his interest and support. Part of this work was supported by the INTAS YSF 01/1-238 grant.

References

[1] The Compact Muon Solenoid (CMS) Technical Proposal, CERN/LHCC 94-38, December 1994.

[2] CMS ECAL Technical Design Report. CERN/LHCC 97-33 CMS TDR4(1977), December 1997.

[3] CMS HCAL Technical Design Report. CERN/LHCC 97-31. CMS TDR2, June 1997.

[4] *"Study of the response of the prototype CMS hadron calorimeter, including magnetic field effects, to pion, electon and muon beams."* V.Abramov et al. CERN CMS NOTE 2000/03. *(See figures 28 and 31 in the paper for example.)*

[5] *"Energy corrections for QCD jets."* S.Abdullin et al. CERN CMS IN 2001/001.

[6] *"Jet Quality and H to bb Mass resolution".* V.Drollinger, Th.Muller. CMS NOTE 2000/073, Section 4.2, page8.

[7] T.Sjostrand. Comp. Phys. Com. 82/1994) 74.

[8] *"Minimum-bias pileup issues in electron-photon HLT studies."* C.Seez. CERN CMS IN 2000/001.

[9] CMSIM user's Guide at www.http://cmsdoc.cern.ch/swsi.html.

[10] *"Jet finding algorithms in heavy ion collisions in CMS"* N.Kruglov et al. CERN CMS TN/96-084.

[11] S.Kunori. http://home.fnal.gov/~kunori/cms_sw/colo_sw/hcal_hits_digi.html.

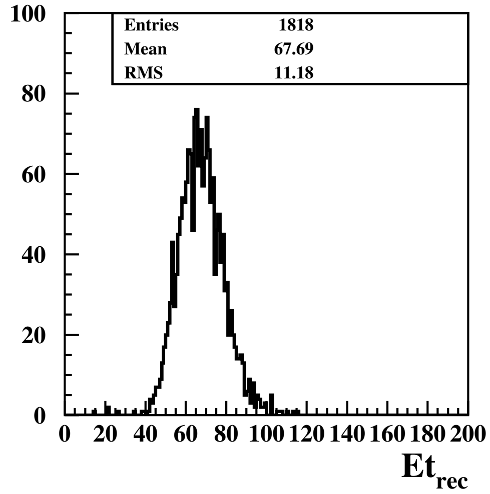

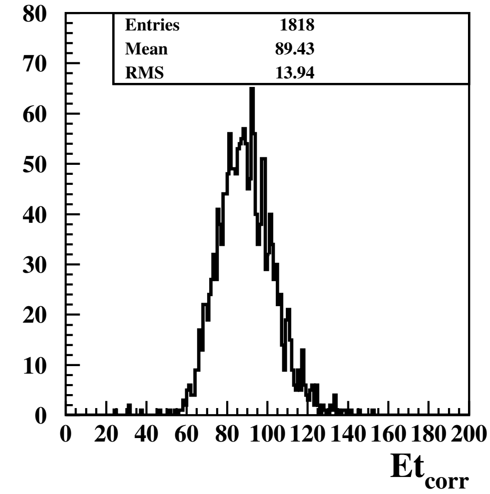

Figure 16: Energy distribution of the reconstructed calorimeter jets associated with the particle jets from Fig.15. Trivial weights $w_i = 1$ were used here to calculate reconstructed jet energy.

Figure 17: The same distribution as in Fig.16 after energy scale corrections were applied.

[12] HCAL TDR. CERN/LHCC 97-31. CMS TDR2, June 1997. *(see Fig.1.26 for passive weights.)*

[13] http://cmsdoc.cern.ch/orca, *"Object Oriented Reconstruction for CMS Analysis"*

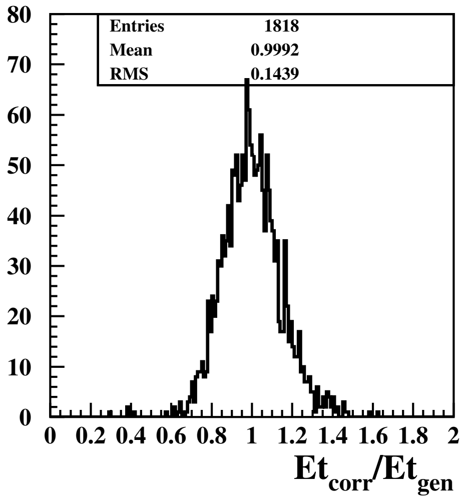

Figure 18: Ratio of the corrected energy of the reconstructed jets to the energy of the generated jets for the same event sample as in Fig.15-17.Jet energy resolution is defined as RMS/Mean of this distribution.

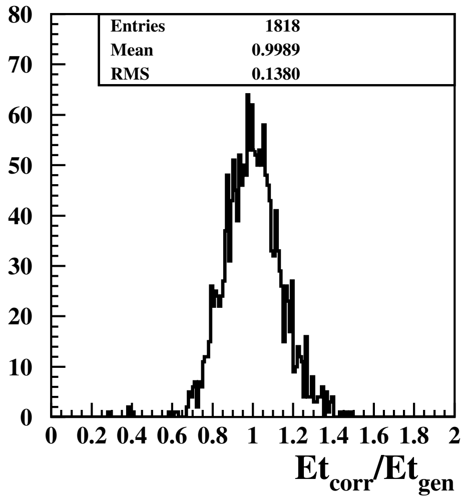

Figure 19: The same distribution as in Fig.18 obtained with the optimum readout readout weights w_i.

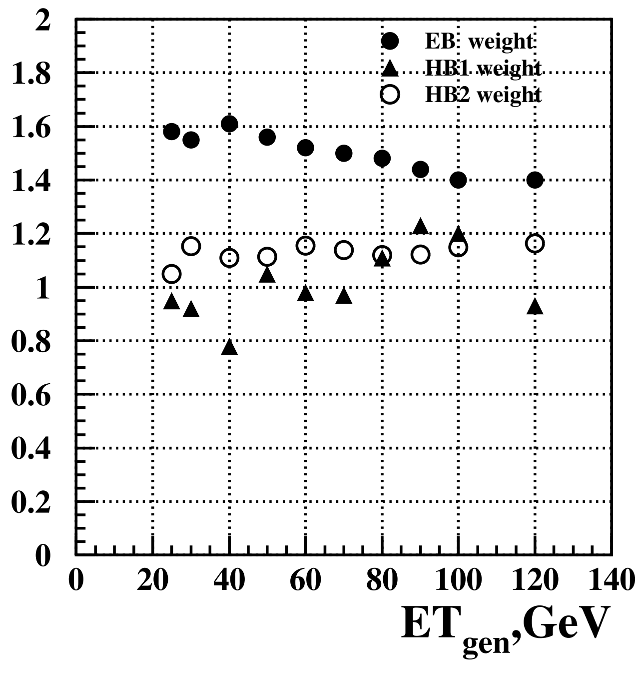

Figure 20: Energy dependence of the optimum weights for $|\eta| < 0.4$.